Nuclear Activity in Galaxies Across Cosmic Time
Proceedings IAU Symposium No. 356, 2019
M. Pović, P. Marziani, J. Masegosa, H. Netzer, S. H. Negu & S. B. Tessema, eds.
doi:10.1017/S1743921320002562

Towards a new paradigm of dust structure in AGN: Dissecting the mid-IR emission of Circinus galaxy

Marko Stalevski[1], Daniel Asmus[2] and Konrad R. W. Tristram[3]

[1]Astronomical Observatory, Volgina 7, 11060 Belgrade, Serbia
email: mstalevski@aob.rs

[2]Dept. of Physics & Astronomy, University of Southampton, SO17 1BJ, Southampton United Kingdom

[3]European Southern Observatory, Casilla 19001, Santiago 19, Chile

Abstract. Recent mid-infrared (MIR) observations of nearby active galactic nuclei (AGN), revealed that their dust emission appears prominently extended in the polar direction, at odds with the expectations from the canonical dusty torus. This polar dust, tentatively associated with dusty winds driven by radiation pressure, is found to have a major contribution to the MIR flux from a few to hundreds of parsecs. One such source with a clear detection of polar dust is a nearby, well-known AGN in the Circinus galaxy. We proposed a phenomenological model consisting of a compact, thin dusty disk and a large-scale polar outflow in the form of a hyperboloid shell and demonstrated that such a model is able to explain the peculiar MIR morphology on large scales seen by VLT/VISIR and the interferometric data from VLTI/MIDI that probe the small scales. Our results call for caution when attributing dust emission of unresolved sources entirely to the torus and warrant further investigation of the MIR emission in the polar regions of AGN.

Keywords. galaxies: individual (Circinus), galaxies: active, galaxies: nuclei, galaxies: Seyfert, infrared: galaxies, radiative transfer, radiation mechanisms: thermal

1. Introduction

In a widely-accepted picture, dust in active galactic nuclei (AGN) is contained around the equatorial plane in a roughly toroidal shape, nicknamed "the dusty torus" (Antonucci 1993; Netzer 2015). However, recent mid-infrared (MIR) interferometric observations revealed that thermal dust emission in AGN appears to be originating dominantly along the polar direction, following the orientation of the ionisation cone, jet, polarisation angle or the accretion disc rotational axis (Hönig *et al.* 2012; López-Gonzaga *et al.* 2016). Furthermore, polar dust emission found to extend out to tens or even hundreds of parsecs (Asmus *et al.* 2016). The orientation of the polar dust emission on large and small scales roughly match, indicating that both might have a same physical origin, namely a dusty wind driven by the radiation pressure on the dust grains close to the sublimation radius. These findings have a potential to lead us towards a new paradigm for the dust structure in AGN.

2. Data

We obtained Circinus images at 8.6 μm and 11.9 μm with the VISIR instrument mounted on the Very Large Telescope (VLT) as part of its science verification after the upgrade (Stalevski *et al.* 2017). We complemented them with archival 10.5 μm and

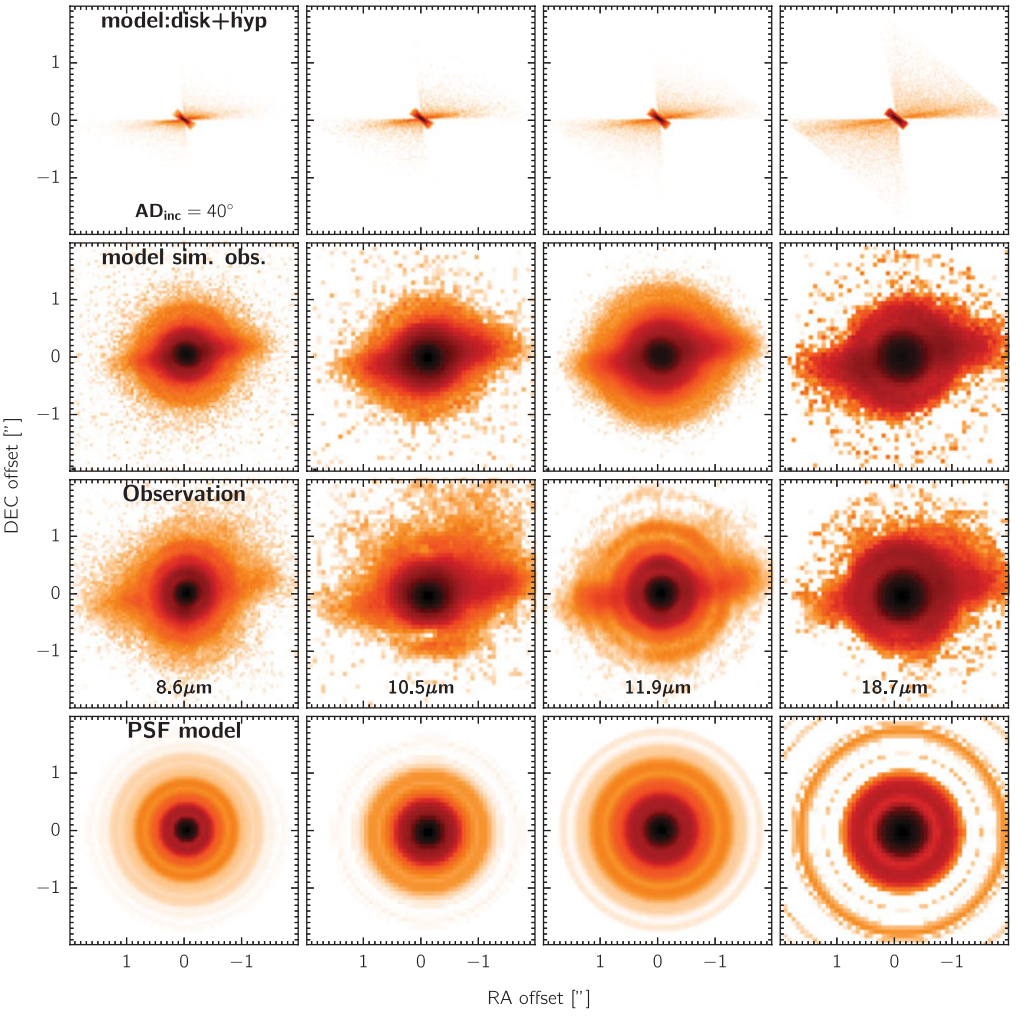

Figure 1. Comparison of the VISIR images of Circinus with the representative model, including foreground extinction. From top to bottom, the rows show: (1) the model images; (2) the model images as they would appear when observed with VISIR; (3) the images of Circinus acquired with VISIR; (4) our approximation of the observed PSF. Adapted from Stalevski *et al.* (2017)

18.7 μm VISIR images. The central 4" $\times$ 4" region of these images is shown in the third row of Fig. 1. A prominent bar-like feature is present in all of them, extending to $\sim$40 pc on both sides of the nucleus, and coinciding with the edge of the ionization cone seen at visible wavelengths on the Western side. Circinus was also observed with the MID-infrared Interferometric instrument (MIDI) at the VLT interferometer between 8 and 13 μm (Tristram *et al.* 2014). For comparison of the model and the data over a wider wavelength range, we also assembled the observed nuclear SED and spectra of Circinus from data available in the literature.

3. Model

The illumination pattern of the ionization cone (brighter toward the western edge) is indicative of the anisotropic emission pattern of the ionizing source. This is supported by the orientation of the inner part of the maser disk, which is roughly perpendicular to the

https://doi.org/10.1017/S1743921320002562 Published online by Cambridge University Press

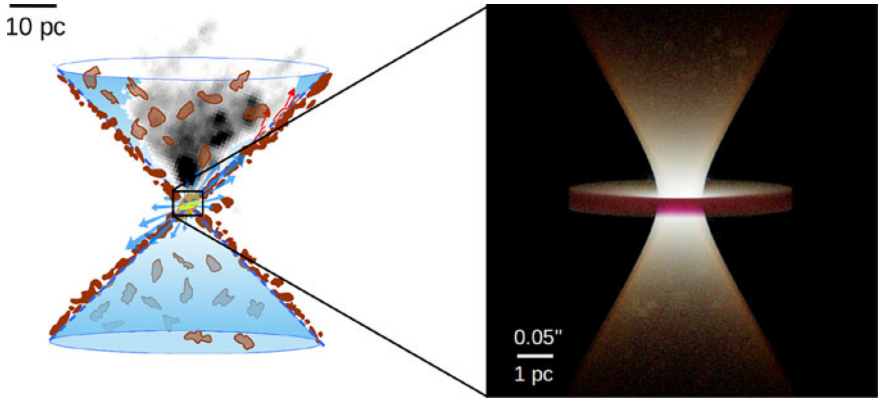

Figure 2. Left: Schematic of our model for the nuclear dust distribution in Circinus consisting of a compact dusty disk and a dusty hollow cone enveloping ionized gas seen in the optical (show in gray scale). The blue arrows illustrate the anisotropic emission pattern of the accretion disk, whose orientation matches the orientation of the inner part of the warped maser disk. Right: zoom into the central region, where our modeling of the MIDI data revealed a thin dusty disk and a dusty wind shaped like a hyperboloid; a colour composite image (in logarithmic scale) of our best model made by mapping the 8, 10 and 13 μm flux images obtained with radiative transfer simulations to the blue, green and red, respectively. Adapted from Stalevski *et al.* (2017) and Stalevski *et al.* (2019)

cone edge. An optically-thick, geometrically-thin accretion disk displays a $\cos\theta$ angular-dependent luminosity profile. Aligned with the inner part of the warped maser disk, such a disk will emit more strongly into or close to the western edge of the cone. If the cone wall is dusty, then the described setup could naturally produce the dusty bar seen in the VISIR image. The opposite side of the cone wall would remain cold and invisible, as the tilted anisotropic accretion disk would emit very little in that direction. Thus, we proposed a model consisting of a geometrically thin disc and a hollow cone (i.e. hyperboloid shell), as depicted in the schematic in Fig. 2. The dust composition and grain size distribution is a mixture of silicates (53%) and graphite (47%) in the disc and only graphite in the polar region, in both cases following the power-law size distribution ($\propto a^{-3.5}$) with grain sizes in the range of $a = 0.1{-}1$ μm. A foreground absorbing screen is applied to all the models to account for extinction by dust in the disc of the host galaxy. To calculate how the above described model would appear in the IR, we employed SKIRT†, a state–of–the–art 3D radiative transfer code based on the Monte Carlo technique (Baes *et al.* 2011; Baes & Camps 2015; Camps & Baes 2015). The photons are propagated through the simulation box following the standard Monte Carlo radiation transfer prescriptions that take into account all the relevant physical processes: anisotropic scattering, absorption and thermal re-emission. At the end of the simulation, images and SEDs of the model can be reconstructed for the comparison with the observations in the entire wavelength range of interest.

4. Results and conclusions

In Fig. 1, we compare the VISIR images of Circinus with the synthetic observations of our representative model, produce by convolution with the instrumental PSF and including background noise and foreground extinction. We see that the simulated model images provide a good match to the observed morphology at all wavelengths.

† http://www.skirt.ugent.be

https://doi.org/10.1017/S1743921320002562 Published online by Cambridge University Press

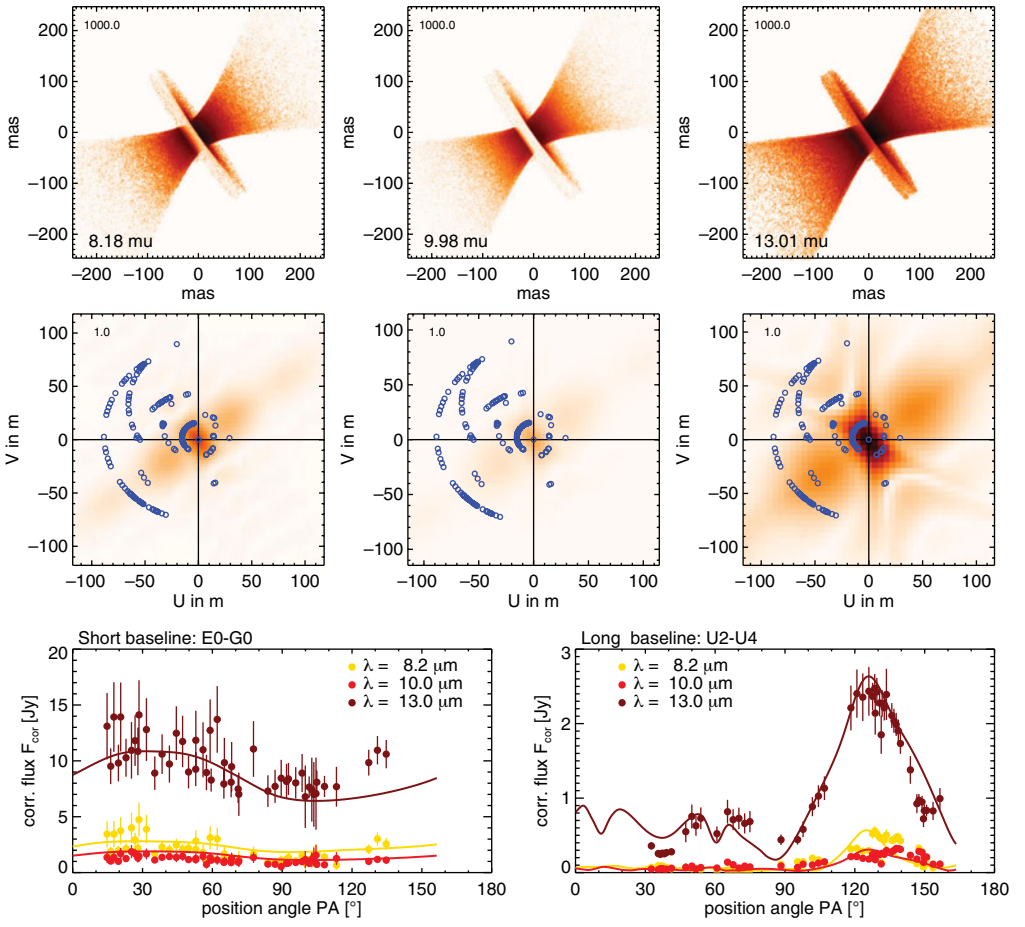

Figure 3. The interferometric diagnostic plots for the best disc+hyperboloid model. From top to bottom, the rows show: (1) The model images at 8, 10 and 13 μm. (2) The Fourier transform of the model surface brightness distribution in the *uv* plane with blue circles marking the positions of the interferometric measurements. (3) The correlated fluxes ($F_{\rm cor}$) of the interferometric measurements (dots) and of the model (lines) as a function of the position angle (PA) of the projected baseline lengths (BL). The signal seen in $F_{\rm cor}$ vs. PA is well reproduced by the model at both short and long baselines and at all wavelengths.

Fig. 3 represents the diagnostic plots we used to compare the model to the MIDI data. This figure contains our disc+hyperboloid model images (first row) and the Fourier transforms of the model surface brightness (second row), but the most important information is in the third row, featuring correlated flux as a function of the position angle, for short and long baselines and at three wavelengths. Here we show correlated fluxes for the two telescope combinations which probe different spatial scales alongn various directions. The correlated fluxes of the short baselines (third row, left panel) probe larger spatial scales. They show a wide minimum at PA $\sim 90°$ indicating extended emission in this direction, which is reproduced by the dusty hyperboloid shell of our model. The correlated fluxes of the long baselines (third row, right panel), which probe smaller scales, have a prominent peak at PA $\sim 125°$. This suggests a very elongated surface brightness of the source, which is in our model reproduced by the dusty disc seen almost edge-on.

In Fig. 4, we compare our VISIR-based model (solid black line) and the MIDI-based models (disc+hyperboloid in dash-dotted red line and clumpy version of the same model

https://doi.org/10.1017/S1743921320002562 Published online by Cambridge University Press

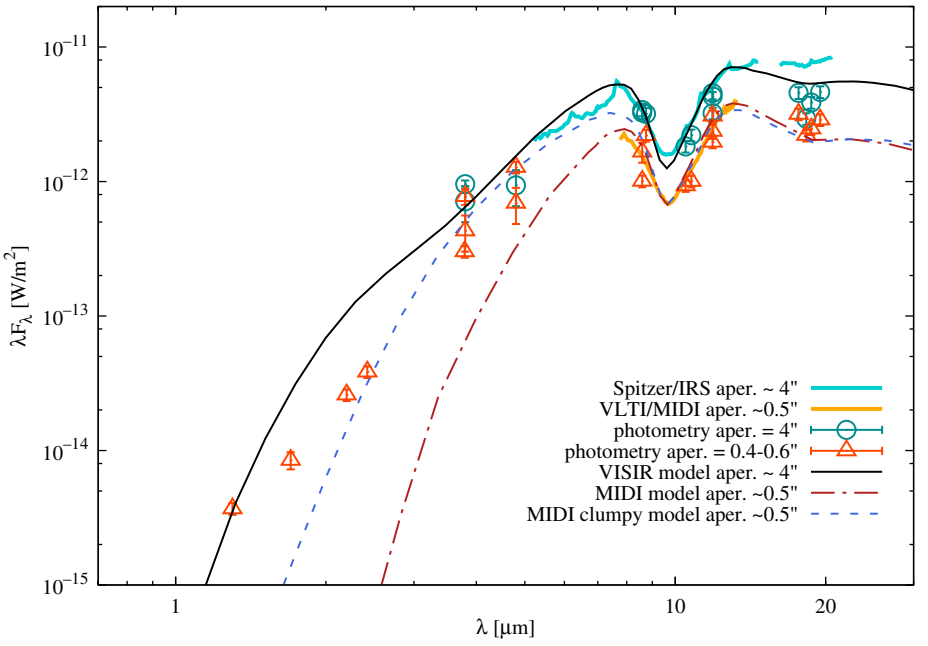

Figure 4. Comparison of the observed SED with the VISIR-based model SED from Stalevski *et al.* (2017) (solid black line), the MIDI-based models from Stalevski *et al.* (2019) (a smooth model in dash-dotted red line and a clumpy model in dashed blue line). Large-scale aperture photometry (4") is shown in green down-pointing triangles, while photometry extracted from apertures comparable or smaller than the resolution limit of VISIR (0.4−0.6") is marked by red up-pointing triangles. The aperture of the Spitzer/IRS spectrum ($\gtrsim 3.6$") is comparable to the total aperture of VISIR in $5.2 - 14.5$ μm range, while significantly larger at longer wavelengths. The MIDI spectrum was extracted using a $\sim 0.54" \times 0.52"$ aperture and hence corresponds to the unresolved nucleus with VISIR. Adapted from Stalevski *et al.* (2019).

in dashed blue line) with the observed SED. For all the observations, we measured the fluxes consistently in a 4" diameter aperture (corresponding to the total VISIR aperture) and a 0.4−0.6" diameter aperture (corresponding to the unresolved core in VISIR and the MIDI total flux spectrum aperture). The clumpy disc+hyperboloid model accounts well for the entire SED, except at the shortest wavelength which are likely contamintated by the host galaxy.

We performed detailed modeling of the Circinus AGN, constructing a model based on observations across a wide range of wavelengths and spatial scales. The model consists of a compact dusty disc and a large-scale hollow dusty cone illuminated by a tilted accretion disc. We showed that this model is able to reproduce well the observed 40 pc scale MIR morphology of Circinus, its entire IR SED and the interferometric observations at all baselines (Stalevski *et al.* 2017 and Stalevski *et al.* 2019). Our results reinforce calls for caution when using the dusty tori models to interpret the IR data of AGN. Further study of polar dust emission in larger samples is necessary to constrain its properties and assess its ubiquity in the whole AGN population.

References

Antonucci, R. 1993, *ARA&A*, 31, 473
Asmus, D., Hönig, S. F., & Gandhi, P. 2016, *ApJ*, 822, 109
Baes, M., Verstappen, J., De Looze, I., *et al.* 2011, *ApJS*, 196, 22
Baes, M. & Camps, P. 2015, *Astronomy and Computing*, 12, 33

https://doi.org/10.1017/S1743921320002562 Published online by Cambridge University Press

Camps, P., & Baes, M. 2015, *Astronomy and Computing*, 9, 20
Hönig, S. F., Kishimoto, M., Antonucci, R., *et al.* 2012, *ApJ*, 755, 149
López-Gonzaga, N., Burtscher, L., Tristram, K. R. W., *et al.* 2016, *A&A*, 591, A47
Netzer, H. 2015, *ARA&A*, 53, 365
Tristram, K. R. W., Burtscher, L., Jaffe, W., *et al.* 2014, *A&A*, 563, A82
Stalevski, M., Asmus, D., & Tristram, K. R. W. 2017, *MNRAS*, 472, 3854
Stalevski, M., Tristram, K. R. W., & Asmus, D. 2019, *MNRAS*, 484, 3334
Tristram, K. R. W., Burtscher, L., Jaffe, W., *et al.* 2014, *A&A*, 563, A82

https://doi.org/10.1017/S1743921320002562 Published online by Cambridge University Press